Published in final edited form as:

Nature. 2009 May 21; 459(7245): 414–418. doi:10.1038/nature08016.

Self-assembly of DNA into nanoscale three-dimensional shapes

Shawn M. Douglas[1,2,3,5], **Hendrik Dietz**[1,2], **Tim Liedl**[1,2], **Bjorn Hogberg**[1,2], **Franziska Graf**[1,2,4,5], and **William M. Shih**[1,2,5]

[1] Department of Cancer Biology, Dana-Farber Cancer Institute, Boston, MA 02115

[2] Department of Biological Chemistry and Molecular Pharmacology, Harvard Medical School, Boston, MA 02115

[3] Department of Genetics, Harvard Medical School, Boston, MA 02115

[4] Department of Pathology, Harvard Medical School, Boston, MA 02115

[5] Wyss Institute for Biologically Inspired Engineering, Harvard University, Cambridge, MA 02138

Abstract

Molecular self-assembly offers a ‘bottom-up’ route to fabrication with subnanometre precision of complex structures from simple components1. DNA has proven a versatile building block2–5 for programmable construction of such objects, including two-dimensional crystals6, nanotubes7–11, and three-dimensional wireframe nanopolyhedra12–17. Templated self-assembly of DNA18 into custom two-dimensional shapes on the megadalton scale has been demonstrated previously with a multiple-kilobase ‘scaffold strand’ that is folded into a flat array of antiparallel helices by interactions with hundreds of oligonucleotide ‘staple strands’19, 20. Here we extend this method to building custom three-dimensional shapes formed as pleated layers of helices constrained to a honeycomb lattice. We demonstrate the design and assembly of nanostructures approximating six shapes — monolith, square nut, railed bridge, genie bottle, stacked cross, slotted cross — with precisely controlled dimensions ranging from 10 to 100 nm. We also show hierarchical assembly of structures such as homomultimeric linear tracks and of heterotrimeric wireframe icosahedra. Proper assembly requires week-long folding times and calibrated monovalent and divalent cation concentrations. We anticipate that our strategy for self-assembling custom three-dimensional shapes will provide a general route to the manufacture of sophisticated devices bearing features on the nanometer scale.

Correspondence and requests for materials should be addressed to W.M.S. (William_Shih@dfci.harvard.edu).

Supplementary Information accompanies the paper on www.nature.com/nature.

Author information Reprints and permissions information is available at npg.nature.com/reprintsandpermissions. The authors declare competing financial interests.

Author contributions S.M.D. designed the monolith and square nut, and provided caDNAno software support; H.D. designed the stacked cross; T.L. designed the railed bridge; B.H. designed the slotted cross; F.G. designed the genie bottle; W.M.S. designed the icosahedron; S.M.D. and W.M.S. developed the honeycomb-pleated-origami design rules; H.D., S.M.D., T.L., B.H., W.M.S. optimized the folding and imaging conditions; all authors collected and analysed data and contributed to preparing the manuscript.

Assembly of a target three-dimensional shape using the honeycomb-pleat-based strategy described here can be conceptualized as laying down the scaffold strand into an array of antiparallel helices (Fig. 1a) where helix *m+1* has a preferred attachment angle to helix *m* of ±120 degrees with respect to the attachment of helix *m−1* to helix *m* (Fig. 1b, c); this angle is determined by the relative register along the helical axes of the Holliday-junction crossovers that connect helix *m+1* to helix *m* versus those that connect helix *m−1 to* helix *m*. Branching flaps are allowed as well (Supplementary Note S1).

The design procedure is analogous to sculpture from a porous crystalline block. Here the block is a honeycomb lattice of antiparallel scaffold helices (Fig. 1d). Complementary staple strands wind in an antiparallel direction around the scaffold strands to assemble B-form double helices that are assigned initial geometrical parameters (that later can be adjusted to account for interhelical repulsion) of 2.0 nm diameter, 0.34 nm/base-pair rise, and 34.3°/base-pair average twist (or 21 base pairs/2 turns). Crossovers between adjacent staple helices are restricted to intersections between the block and every third layer of a stack of planes orthogonal to the helical axes, spaced apart at intervals of 7 base pairs or two-thirds of a turn (Fig. 1c). Crossovers between adjacent scaffold helices are permitted at positions displaced upstream or downstream of the corresponding staple-crossover points by 5 base pairs or a half-turn.

The first steps in the design process are carving away duplex segments from the block to define the target shape, and then introducing scaffold crossovers at a subset of allowed positions so as to create a singular scaffold path that visits all remaining duplex segments. Next, staple crossovers are added at all permitted positions on the shape that are not 5 base pairs away from a scaffold crossover; this exception maintains the local crossover density along any helix-helix interface at roughly one per 21 base pairs. Nicks are introduced into staple helices to define staple strands whose lengths are between 18 and 49 bases inclusive, with an average between 30 and 42 bases. Sometimes staple crossovers are removed at the edges of the shapes to allow adjustment of staple lengths to preferred values. Unpaired scaffold bases often are introduced at the ends of helices to minimize undesired multimerization, or else to accommodate later addition of connecting staple strands that mediate desired multimerization. The final step is to thread the actual scaffold sequence on the target scaffold path to determine the Watson-Crick-complementary sequences of the staple strands.

Design steps and assignment of staple sequences for the shapes presented here were aided by manual rendering of strand diagrams in Adobe Illustrator and by writing *ad hoc* computer programs to produce staple sequences corresponding to those diagrams. This process was very time consuming and error-prone even for trained DNA nanotechnologists. More recently, we have developed caDNAno, a graphical-interface-based computer-aided-design environment for assisting in honeycomb-pleated-origami design21, and have ported all the objects described in this article into this framework (Supplementary Note S2). With caDNAno, an individual with no prior knowledge of programming or DNA structure can complete a short tutorial and then be capable of generating sequences within a day for building a new shape comparable in complexity to the examples demonstrated here.

As with flat DNA origami19, assembly of three-dimensional, honeycomb-pleated DNA origami proceeds in a one-pot reaction, after rapid heating followed by slow cooling, between a scaffold strand and the hundreds of oligonucleotide staple strands that direct its folding into the target shape. Successful folding was observed for a panel of five structural targets (detailed schematics in Supplementary Note S2) each produced by mixing 10 nM scaffold strands derived from the single-stranded genome of the M13 bacteriophage (preparation described in Supplementary Note S1), 50 nM of every oligonucleotide staple strand, purified by reverse-phase cartridge (Bioneer Inc.), buffer and salts including 5 mM Tris, 1 mM EDTA (pH 7.9 at 20°C), 16 mM $MgCl_2$, and subjecting the mixture to a thermal-annealing ramp that cooled from 80°C to 60°C over the course of 80 minutes and then cooled from 60°C to 24°C over the course of 173 hours. Objects were electrophoresed on a 2% agarose gel containing 0.5xTBE and 11 mM $MgCl_2$ at 70 V for four hours cooled by an ice-water bath, monomer bands were excised, DNA was recovered by physical extraction from the excised band, and the objects were imaged using transmission electron microscopy after negative-staining by uranyl formate. The fraction of scaffold strands that were incorporated into monomeric species after folding varied from 7% to 44% for these targets as estimated by ethidium-bromide fluorescence intensity. Gel-purified particles generally were observed to be monodisperse with a homogenous shape (Fig. 2f); defect analysis for a series of related objects can be found elsewhere21.

The five objects displayed in Fig. 2 demonstrate the generality of this honeycomb-pleated origami approach in approximating various three-dimensional shapes. Fig. 2a shows a structure resembling a monolith, assembled in the form of a honeycomb-pleated block as in Fig. 1, except with ten layers instead of three. Particles display the predicted pattern of holes and stripes consistent with a honeycomb lattice of cylinders. Fig. 2b shows a square nut, whose cross section is a block of the honeycomb lattice with an internal pore shaped like a six-pointed star. Fig. 2c shows a structure that resembles a bridge with hand rails. This shape demonstrates that different cross-section patterns can be implemented along the helical axis. Fig. 2d shows a slotted cross, a structure composed of two honeycomb-lattice-based domains that sit at 90 degrees to the other. One domain is H-shaped, the other is O-shaped. The center of the H-domain passes through the slot of the O-domain, and the two domains are connected by a pair of Holliday-junction crossovers derived from the scaffold strand. The 90 degree angle between domains is enforced by steric collisions between the ends of helices on the H-domain and the sides of helices on the O-domain. The fifth particle image for the slotted cross in Fig. 2d shows a defective particle, where the slot in the O-domain can be seen clearly. Fig. 2e shows a stacked cross, where again two domains sit at 90 degrees to the other. One domain is C-shaped, the other domain resembles a pod with a cavity. The pod domain consists of four sub-modules that each are connected to the C-shaped domain by a Holliday-junction crossover derived from the scaffold strand. Upon folding, the sub-modules connect to each other by staple linkages, enforcing a rotation to yield the complete pod domain oriented 90 degrees to the C-module.

For the monolith, an effective diameter of 2.4 nm (±0.1 nm s.d.) per individual double helix was observed (Fig. 2g, h), while for the square nut an effective diameter of 2.1 nm (±0.1 nm s.d.) per individual double helix was observed (Fig. 2i, j). Assuming an unhydrated helical diameter of 2.0 nm (although the hydrodynamic helical diameter has been estimated as 2.2

to 2.6 nm22), this observation suggests the presence of inter-helical gaps produced by electrostatic repulsion8 on the order of 0.1–0.4 nm, significantly less than the 1.0 nm gap size estimated for Rothemund flat origami. This discrepancy likely is related to the roughly two-fold higher density of crossovers present in the honeycomb-pleated origami. Differences in effective helix diameter between architectures may originate in part from staining artifacts (e.g. cavities where large amounts of positively charged stain accumulate; flattening).

Three key determinants for folding of honeycomb-pleated origami were investigated: duration of thermal ramp, divalent-cation concentration, and monovalent-cation concentration. Folding with short thermal ramps (Fig. 3b, lefthand lanes), low concentrations of $MgCl_2$ (Fig. 3d lefthand lanes), or high concentrations of NaCl (Fig. 3f, lefthand lanes) yielded a slowly migrating species upon agarose-gel electrophoresis and grossly misshapen objects as observed by transmission electron microscopy (for example, see Fig. 3c). In contrast, week-long thermal annealing at higher concentrations of $MgCl_2$ combined with low concentrations of NaCl yielded a fast-migrating species upon agarose-gel electrophoresis and well-folded particles as observed by electron microscopy (Fig. 3e), along with lower mobility bands corresponding to multimerized and aggregated objects. The apparent trend was that increasing agarose-gel mobility correlated with improvement of quality of folding as observed by transmission electron microscopy, suggesting that correctly folded structures tend to be more compact than misfolded versions.

Divalent cations thus appear to accelerate the rate of proper folding and increase the amount of undesired aggregation while monovalent cations appear to decelerate the rate of proper folding and decrease the amount of undesired aggregation. Many of the structures require week-long thermal ramps for proper folding, even under idealized divalent- and monovalent-cation concentrations. Divalent cations may accelerate target folding by specific stabilization of Holliday-junction crossovers23 and by nonspecific stabilization of compact DNA24 folding intermediates, although they also may stabilize nontarget aggregates by a similar mechanism. Monovalent-cation binding might compete with divalent-cation binding, and thereby antagonize both target compaction and nontarget aggregation, analogous to how such binding inhibits multivalent-cation-induced DNA condensation25. Folding of simpler DNA-origami structures such as the six-helix-bundle nanotube is much more robust to variations in annealing conditions (Supplementary Note S1); the Rothemund flat origami and these simpler nanotube structures could be folded with 72 minute ramps. Presumably, multilayered structures must traverse more difficult kinetic traps, perhaps due in part to the larger density of crossovers, in part to issues of local folding and unfolding in the confined space between two or more layers of DNA helices, and in part to the difficulties in reaching a high density of DNA in the final folded object, similar to that found in high-pressure virus capsids26.

One of the target shapes presented in Fig. 3 — the genie bottle (strand diagram in Supplementary Note S2) — was folded with two different scaffold sequences. Its full size takes up only 4500 base pairs. One scaffold sequence used for folding was a modified M13 genome with a length of 7308 bases, where 2800 bases of the scaffold strand were left unpaired and dangling from the neck of the bottle (reminiscent of wisps of smoke in TEM

images), while the other scaffold sequence used was the 4733-base forward strand of an expression vector encoding the enhanced green fluorescent protein (**pEGFP-N1**, Clontech). Folding of the same shape under identical conditions gave superior yield with the M13-based scaffold sequence. Some folding success could be achieved with the **pEGFP-N1** scaffold sequence when much higher scaffold and staple concentrations were used. One striking difference between the two scaffold sequences is that the M13 base composition is 43% cytosines and guanines while the **pEGFP-N1** base composition is 53% cytosines and guanines. Higher levels of GC basepairs might lead to a greater incidence of mispairing during folding and a slower rate of unpairing in misfolded intermediates, which could explain why folding was more difficult with the **pEGFP-N1** scaffold sequence. On the other hand, local sequence diversity is potentially greatest at 50% GC content, thus a scaffold sequence with GC content that is very low might not be well-suited for DNA origami. Systematic studies will be required in the future to determine the optimal base composition.

Hierarchical assembly of DNA-origami nanostructures can be achieved by programming staple strands to bridge separate scaffold strands. Fig. 4a shows the stacked cross programmed to polymerize along the long axes of the DNA helices of the pod domain. The scaffold loops on the ends of the object were programmed with a length such that they form properly spaced scaffold crossovers in the presence of bridging staple strands that link the two ends of the objects. This induces head-to-tail polymerization. Shown are filaments that adsorbed on the grid in two different orientations to illustrate the periodic presentation of the C-shaped domain perpendicular to the filament axis at a periodicity of 41 nm (±3 nm s.d. over a 33mer), corresponding to a length per base pair of 0.33 nm (±0.02 nm s.d.).

Fig. 4b shows a wireframe DNA-origami nanostructure whose struts are six-helix-bundle nanotubes (strand diagrams in Supplementary Note S2). A single scaffold strand is folded into a branched tree that links two pairs of half-struts internally to produce a double triangle (Fig. 4b). This operation is repeated twice more with two completely different sets of staple strands, based on cyclic permutation of the same 8100 base scaffold sequence through the architecture of the double-triangle monomer. This produces three chemically distinct double-triangle monomers that vary according to the sequences displayed at various positions. Each double triangle displays ten terminal branches each presenting scaffold and staple sequences that are programmed to pair specifically with five terminal branches each on the two other double triangles (Fig. 4c). When the three species are mixed together, heterotrimers in the shape of a wireframe icosahedron with a diameter of about 100 nm are formed (Fig. 4d, gel in Supplementary Note S1). The majority of particles visualized by transmission electron microscopy have missing struts, due either to incomplete folding or to particle flattening and collapse, commonly seen for spherical or cylindrical particles prepared by negative-stain protocols27.

Previously, scaffolded DNA origami was employed to create flat structures containing dozens of helices and nanotubes containing six helices9, 28, 29. The present work generalizes this method into three-dimensions by folding helices on a honeycomb lattice. Using the graphical-interface computer-aided-design environment caDNAno21, staple sequences for folding newly conceived objects can be generated quickly. Design, acquisition

of commercially synthesized staple strands, thermal folding, and initial transmission-electron-microscopic imaging all can be completed in as little as two weeks.

Improvements in the rate and yield of folding will be critical for enabling the robust assembly of larger and more complicated DNA nanostructures. Potential steps in this direction include enzymatic synthesis for higher quality staple strands, artificial scaffold sequences that are more amenable to robust folding, folding with formamide dilution instead of thermal ramps to decrease thermal damage to the DNA29, and hierarchical assembly with monomer architectures that have been identified as being particularly well-behaved.

Three-dimensional origami structures should expand the range of possible applications by an increased range of spatial positioning that is not accessible by flat structures, including those requiring encapsulation or space-filling functionalities. For example, many natural biosynthetic machines, such as polymerases, ribosomes, chaperones, and modular synthases use three-dimensional scaffolding to control assembly of complex products. Similar capabilities for synthetic machines thus are more accessible with this convenient, generalizable facility to fabricate custom-shaped three-dimensional structures from DNA.

Supplementary Material

Refer to Web version on PubMed Central for supplementary material.

Acknowledgments

We thank Xingping Su for assistance in cloning M13-based scaffold sequences and Gaelen Hess for pilot studies on the railed-bridge design. This work was supported by a Claudia Adams Barr Program Investigator grant, a Wyss Institute for Biologically Inspired Engineering at Harvard grant, and an NIH New Investigator grant (1DP2OD004641-01) to W.M.S., Humboldt Fellowship to H.D., Deutscher Akademischer Austauschdienst (DAAD) Fellowship to T.L., and Swedish Science Council (Vetenskapsrådet) Fellowship to B.H.

References

1. Whitesides GM, Mathias JP, Seto CT. Molecular self-assembly and nanochemistry: a chemical strategy for the synthesis of nanostructures. Science. 1991; 254:1312–1319. [PubMed: 1962191]
2. Seeman NC. Nucleic acid junctions and lattices. J Theor Biol. 1982; 99:237–247. [PubMed: 6188926]
3. Fu TJ, Seeman NC. DNA double-crossover molecules. Biochemistry. 1993; 32:3211–3220. [PubMed: 8461289]
4. Li XJ, Yang XP, Qi J, Seeman NC. Antiparallel DNA double crossover molecules as components for nanoconstruction. J Am Chem Soc. 1996; 118:6131–6140.
5. Seeman NC. DNA in a material world. Nature. 2003; 421:427–431. [PubMed: 12540916]
6. Winfree E, Liu F, Wenzler LA, Seeman NC. Design and self-assembly of two-dimensional DNA crystals. Nature. 1998; 394:539–544. [PubMed: 9707114]
7. Yan H, Park SH, Finkelstein H, Reif JH, LaBean TH. DNA-templated self-assembly of protein arrays and highly conductive nanowires. Science. 2003; 301:1882–1884. [PubMed: 14512621]
8. Rothemund PW, et al. Design and characterization of programmable DNA nanotubes. J Am Chem Soc. 2004; 126:16344–16352. [PubMed: 15600335]
9. Mathieu F, et al. Six-helix bundles designed from DNA. Nano Lett. 2005; 5:661–665. [PubMed: 15826105]

10. Liu D, Park SH, Reif JH, LaBean TH. DNA nanotubes self-assembled from triple-crossover tiles as templates for conductive nanowires. Proc Natl Acad Sci USA. 2004; 101:717–722. [PubMed: 14709674]
11. Yin P, et al. Programming DNA tube circumferences. Science. 2008; 321:824–826. [PubMed: 18687961]
12. Goodman RP, et al. Rapid chiral assembly of rigid DNA building blocks for molecular nanofabrication. Science. 2005; 310:1661–1665. [PubMed: 16339440]
13. Chen JH, Seeman NC. Synthesis from DNA of a molecule with the connectivity of a cube. Nature. 1991; 350:631–633. [PubMed: 2017259]
14. Zhang Y, Seeman NC. The construction of a DNA truncated octahedron. J Am Chem Soc. 1994; 116:1661–1669.
15. He Y, et al. Hierarchical self-assembly of DNA into symmetric supramolecular polyhedra. Nature. 2008; 452:198–201. [PubMed: 18337818]
16. Zhang C, et al. Conformational flexibility facilitates self-assembly of complex DNA nanostructures. Proc Natl Acad Sci USA. 2008; 105:10665–10669. [PubMed: 18667705]
17. Shih WM, Quispe JD, Joyce GF. A 1.7-kilobase single-stranded DNA that folds into a nanoscale octahedron. Nature. 2004; 427:618–621. [PubMed: 14961116]
18. Whitesides GM, Grzybowski B. Self-assembly at all scales. Science. 2002; 295:2418–2421. [PubMed: 11923529]
19. Rothemund PW. Folding DNA to create nanoscale shapes and patterns. Nature. 2006; 440:297–302. [PubMed: 16541064]
20. Yan H, LaBean TH, Feng L, Reif JH. Directed nucleation assembly of DNA tile complexes for barcode-patterned lattices. Proc Natl Acad Sci USA. 2003; 100:8103–8108. [PubMed: 12821776]
21. Douglas SM, et al. Rapid prototyping of three-dimensional DNA-origami shapes with caDNAno. Nucleic Acids Research. accepted (2009).
22. Mandelkern M, Elias JG, Eden D, Crothers DM. The dimensions of DNA in solution. J Mol Biol. 1981; 152:153–161. [PubMed: 7338906]
23. Diekmann S, Lilley DMJ. The anomalous gel migration of a stable cruciform: temperature and salt dependence, and some comparisons with curved DNA. Nucleic Acids Research. 1987; 15:5765–5774. [PubMed: 3039465]
24. Budker V, Trubetskoy V, Wolff JA. Condensation of nonstoichiometric DNA/polycation complexes by divalent cations. Biopolymers. 2006; 83:646–657. [PubMed: 16977627]
25. Hibino K, et al. Na+ more strongly inhibits DNA compaction by spermidin(3+) than K+ Chemical Physics Letters. 2006; 426:405–409.
26. Garcia HG, et al. Biological consequences of tightly bent DNA: the other life of a macromolecular celebrity. Biopolymers. 2007; 85:115–130. [PubMed: 17103419]
27. Harris JR, Gerber M, Gebauer W, Wernicke W, Markl J. Negative stains containing trehalose: application to tubular and filamentous structures. Microscopy and microanalysis. 1996; 2:43–52.
28. Douglas SM, Chou JJ, Shih WM. DNA-nanotube-induced alignment of membrane proteins for NMR structure determination. Proc Natl Acad Sci USA. 2007; 104:6644–6648. [PubMed: 17404217]
29. Jungmann R, Liedl T, Sobey TL, Shih W, Simmel FC. Isothermal assembly of DNA origami structures using denaturing agents. J Am Chem Soc. 2008; 130:10062–10063. [PubMed: 18613687]

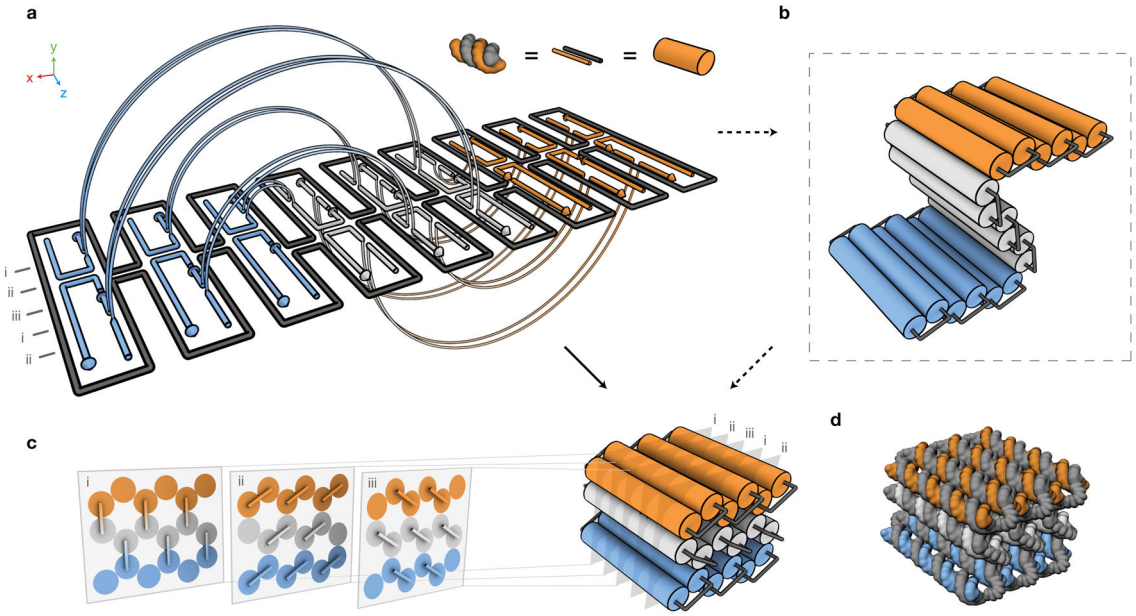

Figure 1. Design of three-dimensional DNA origami

a, Double helices comprised of scaffold (grey) and staple strands (orange, white, blue), run parallel to the z-axis to form an unrolled two-dimensional schematic of the target shape. Phosphate linkages form crossovers between adjacent helices, with staple crossovers bridging different layers shown as semi-circular arcs. **b**, Cylinder model of a half-rolled conceptual intermediate. Cylinders represent double helices, with loops of unpaired scaffold strand linking the ends of adjacent helices. **c**, Three-dimensional cylinder model of folded target shape. Honeycomb arrangement of parallel helices is shown in cross-sectional slices (i–iii) parallel to the x–y plane spaced apart at 7 base-pair intervals repeating every 21 base pairs. All potential staple crossovers are shown for each cross-section. **d**, Atomistic DNA model of shape from **c**.

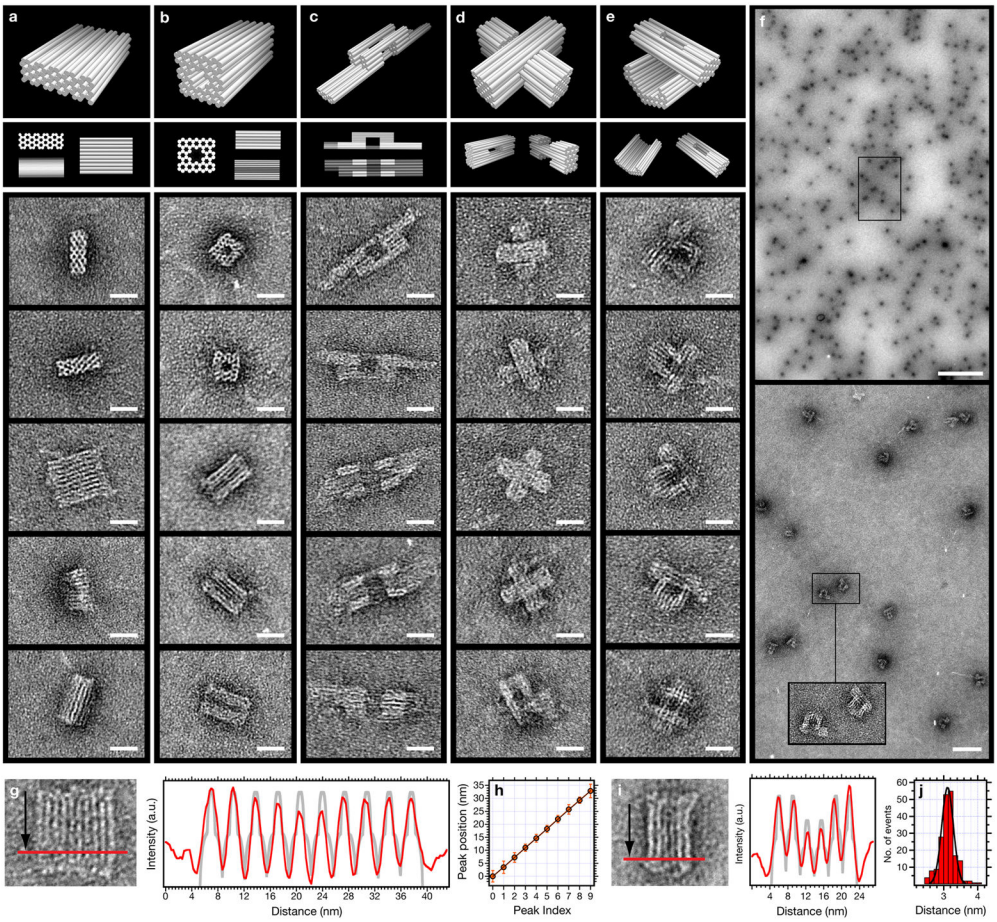

Figure 2. Three-dimensional DNA origami shapes

First and second rows, perspective and projection views of cylinder models, with each cylinder representing a DNA double helix. **a**, monolith. **b**, square nut. **c**, railed bridge. **d**, slotted cross. **e**, stacked cross. Rows 3–7, transmission electron microscope (TEM) micrographs of typical particles. For imaging, samples were adsorbed (5 min) onto glow-discharged grids pre-treated with 0.5 M $MgCl_2$, stained with 2% uranyl formate, 25mM NaOH (1 min), and visualized with an FEI Tecnai T12 BioTWIN at 120 kV. **f**, Field of homogeneous and monodisperse stacked-cross particles. **g**, Integrated-intensity profile (red) of line orthogonal to the longitudinal axis of typical monolith particle, with expected profile (grey) assuming a simple homogeneous cylinder model. **h**, Gaussian-fitted average peak positions (circles) in such integrated-line profiles for twenty different monolith particles as a function of peak index. The observed average peak-to-peak distance was 3.65 nm (±0.2 nm s.d., ±0.01 nm s.e.m.). This peak-to-peak distance should correspond to 1.5 times the effective diameter *d* of individual double helices in the monolith structure, hence *d*=2.4 nm. Solid line: linear fit with a slope of 3.65 nm from peak to peak, corroborating equidistant arrangement of helices across the entire particle width. Error bars (red) indicate mean width of the peaks. Slightly higher variations in peak width at the edges of the particles are most likely due to frayed edges (*cf*. particles in **a**, **g**). **i**, Analysis as in **h** repeated for the square-nut shape. **j**, Histogram of Gaussian-fitted peak-to-peak distances as found for the square-

nut particles, with the mean value at 3.18 nm (±0.2 nm s.d., ±0.01 nm s.e.m.), indicating an effective diameter of 2.1 nm per individual double helix. Scale bars: **a–e**: 20 nm; **f**: 1 μm (top), 100 nm (bottom).

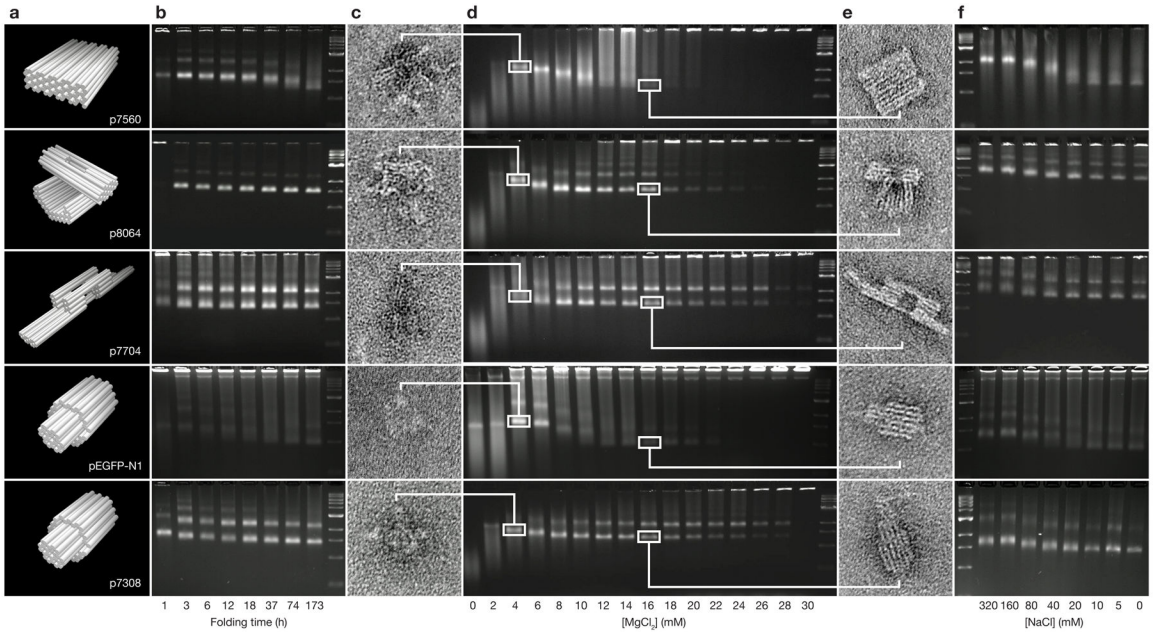

Figure 3. Gel and TEM analysis of folding conditions for three-dimensional DNA origami

a, Cylinder models of shapes: monolith, stacked cross, railed bridge, and two versions of genie bottle, with corresponding scaffold sequences. **b**, Shapes were folded using different thermal-annealing ramps (1.2 h: 95°C to 20°C at 1.6 min/°C; 3 h, 6 h, 12 h, 18 h, 37 h, 74 h, 173 h: 80°C to 60°C at 4 min/°C, followed by 60°C to 24°C at 5, 10, 20, 30, 60, 120, or 280 min/°C, respectively) in 5 mM Tris, 1 mM EDTA, and 16 mM $MgCl_2$ and analyzed by gel electrophoresis (2% agarose, 0.5 × TBE, 11 mM $MgCl_2$). **c–e**, TEM and gel analysis of influence of $MgCl_2$ concentration on folding quality. **c**, The fastest-migrating bands in the 4 mM $MgCl_2$ lanes were purified and imaged, revealing gross folding defects. **d**, Shapes were folded with a 173 h ramp in 5 mM Tris, 1 mM EDTA, and $MgCl_2$ concentrations varying from 0 to 30 mM. **e**, As in **c**, leading bands were purified from the 16 mM $MgCl_2$ lanes and found to exhibit higher-quality folding when analyzed by TEM. **f**, Excess NaCl inhibits proper folding. Shapes were folded with 173 h ramp in 5 mM Tris, 1 mM EDTA, 16 mM $MgCl_2$, and varying NaCl concentrations.

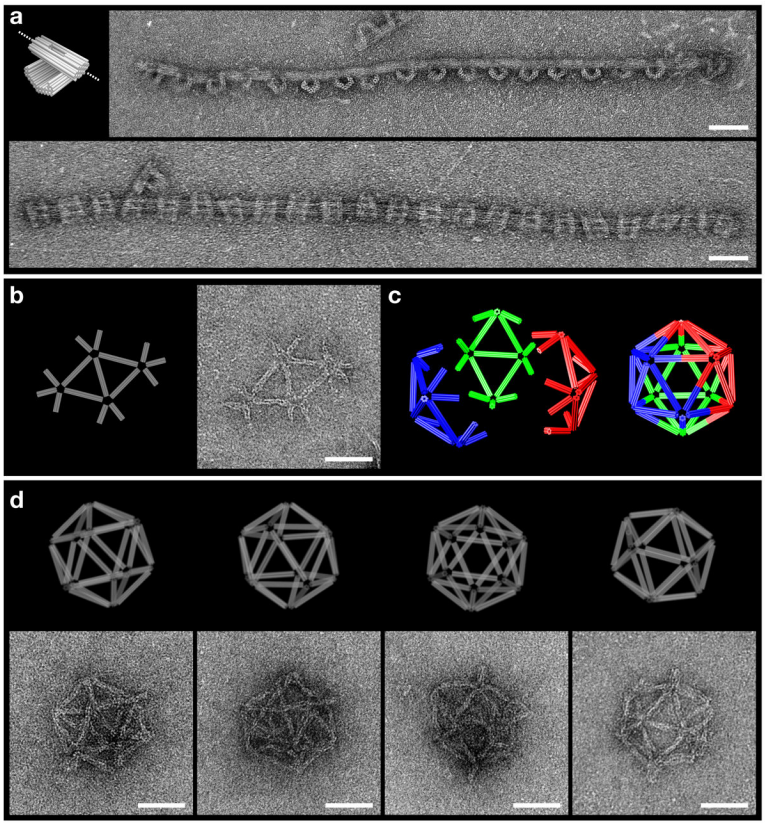

Figure 4. Two-step hierarchical assembly of larger three-dimensional structures and polymers

a, Cylinder model of stacked-cross monomer (Fig. 2e), with dotted line indicating direction of assembly. Typical TEM micrographs showing stacked cross polymers. Purified stacked-cross samples were mixed with a 5-fold molar excess of connector staple strands in the presence of 5 mM Tris, 1 mM EDTA, 16 mM $MgCl_2$ at 30°C for 24 hours. Monomers were folded in separate chambers, purified, and mixed with connector staple strands designed to bridge separate monomers. **b**, Cylinder model and transmission electron micrograph of a double-triangle shape comprised of 20 six-helix bundle half-struts. **c**, Heterotrimerization of the icosahedra was done with a 1:1:1 mixture of the three unpurified monomers at 50°C for 24 hours. **d**, Orthographic projection models and TEM data of four icosahedron particles. Scale bars: 100 nm.